Laser Phys. Lett. **4**, No. 8, 560–571 (2007) / **DOI** 10.1002/lapl.200710021

Abstract: Titanium-doped sapphire is one of the most prominent laser materials and is appreciated for its excellent heat conductivity and broadband gain spectrum, allowing for a wide wavelength tunability and generation of ultrashort pulses. As one of the hardest materials, it can also serve as a model system for the fabrication of optical waveguide structures in dielectric crystalline materials and applications in integrated optics. In this paper, we review the recent approaches towards gain and laser operation in Ti:sapphire optical waveguides, including epitaxial growth, surface micro-structuring, and in-depth refractive-index modifications. Several methods including pulsed laser deposition, reactive ion etching, ion in-diffusion, light-ion implantation, and femtosecond-laser irradiation are presented and the results with respect to obtained refractive-index profiles, waveguide propagation losses, and laser performance are discussed.

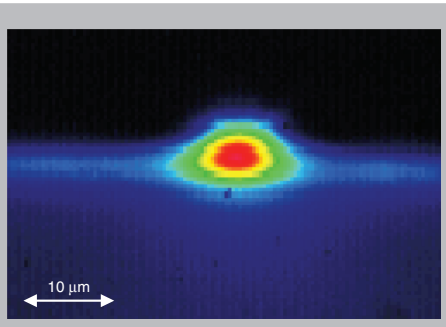

Fluorescence emission profile from a Ti:Sapphire rib waveguide with depth of 5 μm and a width of 10 μm

Ti:Sapphire waveguide lasers◇

M. Pollnau, [1,*] *C. Grivas,* [2] *L. Laversenne,* [3] *J.S. Wilkinson,* [2] *R.W. Eason,* [2] *and D.P. Shepherd* [2]

[1] Integrated Optical Micro Systems Group, MESA+ Research Institute, University of Twente, P.O. Box 217, NL-7500 AE Enschede, The Netherlands
[2] Optoelectronics Research Centre, University of Southampton, Southampton SO17 1BJ, United Kingdom
[3] Laboratoire Multimatériaux et Interfaces, UMR 5615 CNRS, Université Claude Bernard Lyon 1, F-69622 Villeurbanne, France

Received: 19 February 2007, Accepted: 21 February 2007
Published online: 27 February 2007

Key words: sapphire; titanium doping; planar waveguide; channel waveguide; waveguide laser; pulsed laser deposition; reactive ion etching; ion in-diffusion; ion beam implantation; femtosecond laser writing; refractive-index profile; waveguide propagation losses

PACS: 42.79.Gn, 42.70.Hj, 42.55.Rz, 42.60.Jf, 78.20.Ci, 81.40.Wx

1. Introduction

Transition-metal-doped materials exhibiting $3d \leftrightarrow 3d$ electronic transitions are useful as broadly tunable laser sources and for the generation of ultrashort pulses, due to strong homogeneous broadening of the gain bandwidth by interaction with lattice vibrations. Thus far, trivalent titanium-doped sapphire (Al_2O_3:Ti^{3+}, hereafter called Ti:Sapphire) [1] has been the most commercially successful of these vibronic lasers, allowing continuous-wave tunability from $\sim 670-1100$ nm and the generation of pulses as short as ~ 5 fs [2]. Ti:Sapphire lasers are typically pumped by argon-ion or frequency-doubled diode-pumped solid-state lasers with powers of several Watts. Although laser thresholds as low as $\sim$ 100 mW have been demonstrated in the laboratory [3], in general thresholds are much higher, requiring the use of expensive pump sources. This has prompted work on creating Ti:Sapphire waveguides in order to reduce the average spot size in the gain media and thereby lower the laser threshold. Several waveguide fabrication techniques have been used including pulsed laser deposition [4–6], also in combination with reactive ion etching [7] or Ar-ion milling [8,9], proton implantation [10,11], femtosecond-laser writing [12], ion in-diffusion [13,14], Ti and O implantation [15], and crystal fiber growth [16].

In theory, waveguides with cross-sectional areas of the order of λ^2 are feasible, whereas the reported mode size in a bulk Ti:Sapphire laser exhibiting a 100 mW threshold was $\sim$ 8 μm [3], suggesting that considerable improve-

* Corresponding author: e-mail: m.pollnau@ewi.utwente.nl
◇ Invited article

ments should be possible. However, the bulk Ti:Sapphire laser operated efficiently with just a 1% output coupling, indicating very low overall losses, and any waveguide wishing to take advantage of a small mode size will also need to have low losses to see a significant threshold advantage. Besides the possibility of low laser thresholds, the waveguide geometry offers the opportunity of integrating devices with the laser for tuning or mode-locking, e.g. through butting of a saturable absorber reflector for a high-repetition rate, compact femtosecond-laser source [17], and of integrating with other waveguide circuits, e.g. for the purposes of a sensing device that utilizes the large Ti:Sapphire bandwidth. Furthermore, the waveguide geometry allows us to collect larger amounts of broadband luminescence in a fundamental output mode, making a Ti:Sapphire waveguide an interesting light source for white-light interferometry [18].

In this paper, we review the progress made to date in the production of Ti:Sapphire waveguide lasers, indicating the current technological issues, and discussing possible future directions. Following this short introduction, the paper is set out as follows: firstly, we discuss the fabrication techniques that have been used to make Ti:Sapphire waveguides in the planar and channel format; we then discuss the optical characteristics of those waveguides and the laser performances obtained to date; and finally we make our concluding remarks.

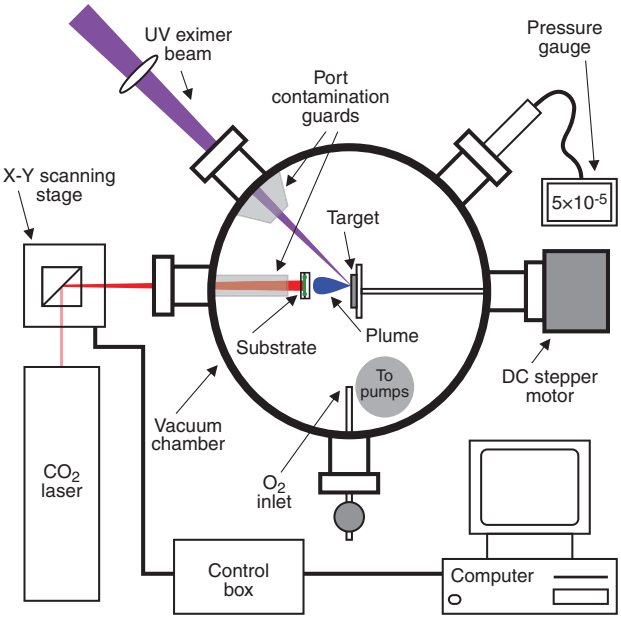

Figure 1 (online color at www.lphys.org) Schematic of a pulsed laser deposition chamber, showing target and substrate mounting and rotation capability. For this particular chamber, substrate heating is via a scanned CO_2 laser beam. Other chambers usually adopt alternative conductive heating schemes

2. Waveguide fabrication methods

Waveguide fabrication techniques fall into two broadly dissimilar categories: those that yield a higher-index waveguiding region *inside* an existing substrate material, producing in general a graded-index guided structure, and those that grow a waveguide layer *onto* a substrate, which yield in general a step-index guide. Examples of the former technique include ion exchange or implantation, in- or out-diffusion, or direct writing using beams of electrons, ions, or photons. All of these techniques are not universally applicable to all host materials however, and undesirable complications exist for some techniques that limit amongst other things, the guide depth and resultant numerical aperture (NA) achievable, restrictions on guided polarization, longevity, and operational temperature limitations, introduction of defects or other undesirable loss mechanisms, and finally the inevitable complications and cost of some of the multi-step processing procedures. These limitations not withstanding however, the technique of titanium in-diffusion, for example in $LiNbO_3$, has been developed for more than 20 years and has now achieved a level of routine perfection that yield waveguides with losses in the $0.01 - 0.1$ dB/cm region.

Examples of the latter technique, which fall under the headings of physical vapor transport and chemical vapor deposition (CVD), include heating and vaporization of a material, sputtering, low-pressure, plasma- and laser-enhanced CVD, liquid phase epitaxy (LPE), molecular beam epitaxy (MBE), and pulsed laser deposition (PLD). Once again, restrictions and limitations apply, and deposition rates for some techniques can be low (< 1 μm per hour), the elements that can be deposited may be restricted by the requirement for undesirable or toxic precursor gases, ultra-high vacuum can be required, and some techniques such as MBE, while capable of precision growth at the level of single atomic layers, require a large initial capital cost of order \$1 M.

Provided that the deposited film exhibits a larger refractive index than the substrate material on which the film is deposited, these methods yield planar waveguides. In combination with surface structuring methods like reactive ion etching (RIE) [7] and Ar-ion milling [8], rib- or ridge-type channel waveguides can be obtained.

2.1. Pulsed laser deposition

It is within this background context that PLD has established itself as a flexible, versatile, fast, and relatively cost-effective technique that can grow a wide range of materials in single layer, multi-layer, graded and step-index, with additional capping or isolation layers.

The PLD apparatus shown in Fig. 1, illustrates a typical set-up for deposition of a single waveguide layer onto a substrate material. The vacuum chamber, of typical dimensions perhaps 30 cm in diameter, does not need to be UHV,

and typical operating pressures (often using oxygen as an ambient background gas) are of order 0.01 mbar. A UV laser which is usually an excimer operating at either 193, 248, or 308 nm produces pulses of duration ~ 10 ns at a repetition rate of ~ 10 Hz, with individual pulse energy between $100 - 500$ mJ. These are focused onto target material (the material to be replicated as the final waveguide material), which is in the form of a rod or pellet, and can be amorphous, sintered, or ideally a single crystal. The laser pulses are loosely focused to an energy density of order $1 - 10$ J/cm^2 onto the rotating target, at an angle of incidence typically of $45°$. The resultant plasma (which contains both electrons, ions, neutrals, and larger scale molecular clusters) is incident on the substrate which is usually placed a distance of a few cm from the target surface. Substrates are almost always heated to temperatures of typically one half of their melting temperature, for example ~ 1000°C for sapphire, either using a conventional resistive block heater, or more flexibly via a CO_2 laser heater as shown in Fig. 1.

Deposition rates can be high, of order > 10 μm per hour for growth of materials such as sapphire, permitting fast growth and rapid systematic investigation of optimum waveguide fabrication parameters. If additional targets are used, as in a carrousel arrangement, multilayer, capped, or clad waveguides can be grown, and doped, off-stoichiometric, and other more exotic variants of deposition can be investigated. Crystal structures can be grown that are difficult or impossible to source commercially as bulk samples, and one-off growth runs can yield results very rapidly in comparison to other rival techniques. To date, we have grown homoepitaxial films of sapphire on sapphire that exceed depths of 100 μm, with a crystal quality that rivals bulk material.

For the growth of Ti:Sapphire layers, control of the valence state of the dopant titanium is of particular importance. A prerequisite for the development of laser devices is the maintenance of the Ti^{3+} state and the minimization of the tetravalent titanium (Ti^{4+}), as the latter is responsible for parasitic absorption and subsequent limitations on the laser performance. Control of the titanium valence state in the PLD-produced waveguides was achieved via optimization of deposition parameters such as background pressure and substrate temperature. Films were grown on undoped sapphire substrates held at a temperature of ~ 975°C, in an argon atmosphere of 3×10^{-4} mbar, from single-crystal Ti:Sapphire targets with a doping level of 0.12 wt% Ti_2O_3 [4]. Ablation was carried out using a KrF excimer laser (248 nm, pulse duration ~ 20 ns) operated at 25 Hz and focused to an energy density of 4 J/cm^2 on the target. Quartz has also been used as a substrate [6], however, due to the tendency of this material to break at elevated temperatures, it was not further considered for the depositions. The degree of crystal perfection and incorporation of the titanium in the films was comparable with commercial bulk targets. Moreover, XRD analysis showed that the Ti^{3+} was incorporated substitutionally for the Al^{3+} in the correct lattice position [4].

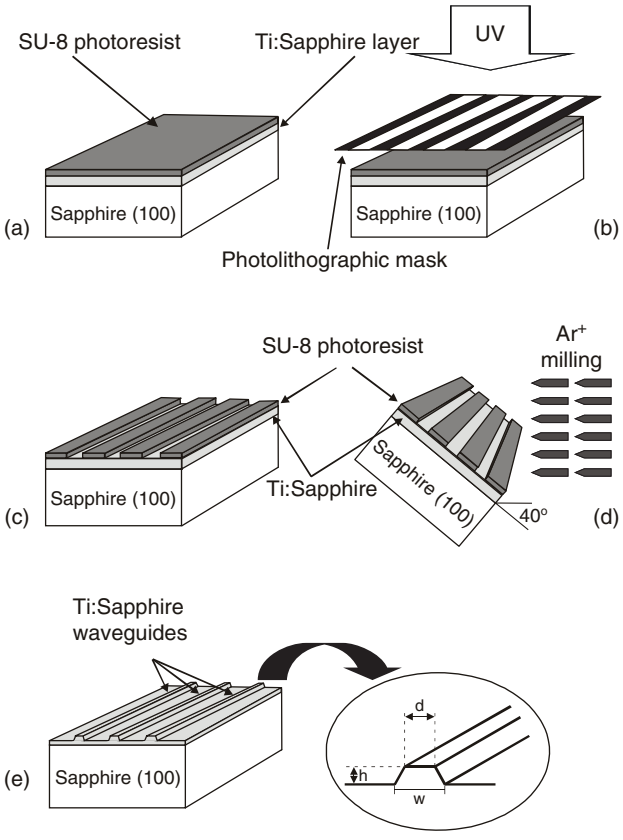

Figure 2 Schematic of the rib fabrication steps in Ti:Sapphire films. (a) Application of a negative photoresist on top of a Ti:Sapphire layer by spin coating. (b) Exposure to UV light (mask aligner). (c) Development to produce stripped patterns of photoresist with a rib shape. (d) Ion beam milling to etch the uncovered Ti:Sapphire surfaces. (e) Removal of the photoresist remnants to obtain rib structures. The inset shows details of the resulting structures. (Figure taken from [8])

2.2. Reactive ion etching and Ar-ion milling

Once surface planar waveguides of good quality are at hand, surface micro-structuring methods such as reactive ion etching [7], Ar-ion milling [8], wet chemical etching [19], or direct laser ablation [20] can be employed in order to fabricate surface channel waveguides. While direct laser ablation has as yet not led to satisfactory results and wet chemical etching requires further improvement before suitable structures can be obtained, reactive ion etching and Ar-ion milling have resulted in well-controlled channel waveguide structures in Ti:Sapphire layers. Subsequently, the obtained rib- or ridge-type waveguide can be buried by overgrowing the sample with an additional layer of the substrate or another material [8].

RIE is a well-established method for patterning semiconductor materials. In recent years, this method was investigated for the fabrication of micro-structures in

Ti:Sapphire [21] and sapphire [22, 23]. We investigated the suitability of RIE and the structural properties of the etched areas in c-cut sapphire substrates [7]. We defined a spin-coated polyimide mask of 12- to 25-μm thickness, which was structured by laser ablation. RIE was performed in a $1:1$-BCl_3:Cl_2 atmosphere at 2- to 3-mTorr pressure by use of an inductive plasma system (STS Multiplex ICP) at 800 W of inductive power. The flow rate of each of the gaseous mixture components was between 10 and 50 sccm. During the process, the sample was maintained at a constant temperature of approximately $20°$C. The etch rate of the sapphire was between 45 and 60 nm/min and the best etch selectivity between the sapphire and the mask was 1:3.5. The structures obtained by this procedure were investigated by profilometry and scanning electron microscopy. Rib heights between 1.2 and 5 μm were obtained. Atomic force microscopy measurements showed that the roughness of the sapphire substrates was lowered from an rms value of 15.9 nm to an rms value of 3.7 nm for the etched regions. The same experimental conditions were used for the RIE of a PLD-grown Ti:Sapphire planar waveguide. We have structured channels of 9-mm length, ~ 1.4-μm depth, and ~ 15-μm width by reactive ion etching (RIE) in a 10-μm-thick Ti(0.1%):sapphire planar waveguide.

Significant improvement was obtained by use of photolithographic patterning and subsequent Ar-ion milling [8]. A 10-μm thick layer of negative photoresist (SU-8) was applied on the top of the PLD-grown Ti:Sapphire waveguide (Fig. 2a) and then was photolithography patterned using a chromium mask and irradiation from a UV lamp (Figs. 2b and 2c). Subsequently, the sample was mounted on a rotating holder and Ar-ion milling was used (Fig. 2d) to etch the exposed parts of the waveguide to produce an array of 5-μm deep Ti:Sapphire ribs with widths w varying from 6 to 16 μm separated by 100 μm (Fig. 2e). As shown in the inset in Fig. 2, the ribs had a trapezoidal profile. The width at the top of the structure d was 60% of the corresponding value w at the base for the $w = 14$-μm rib. The etch rate of the Ti:Sapphire and the SU-8 photoresist using a 500-V neutralized Ar-ion beam with an ion density of 0.9 mA/cm^2 in a background pressure 2×10^{-6} mbar and at an exposure angle of $40°$ were 13 and 24 nm/min, respectively. The exposure angle in the milling process has an impact on the width ratio (d/w) in a way that higher angles lead to more inclined side faces. Then a 5-μm-thick sapphire clad layer was deposited by PLD to reduce scattering losses.

Besides these channel-waveguide fabrication methods which start from an actively-doped planar waveguide deposited onto an undoped substrate, planar and especially channel waveguides can also be fabricated directly inside a Ti:Sapphire bulk crystal. These methods will be described in the following subsections.

2.3. Ion in-diffusion

Diffusion of titanium into lithium niobate is a well-known method to fabricate high-quality optical waveguides, and much sophisticated work has been carried out on combining this technique with rare-earth in-diffusion to realize multifunctional lasers [24,25]. Following this approach, titanium has been diffused into pure sapphire to achieve both a refractive-index elevation, and hence waveguides, and the active Ti:Sapphire medium, and hence Ti:Sapphire waveguide lasers, with a view to further device integration. Typically, Ti:Sapphire in-diffused waveguides are fabricated by depositing 5-μm-wide, 270-nm-thick stripes of titanium oxide onto c-cut sapphire wafers, using vacuum evaporation from a powdered Ti_2O_3 source and conventional photolithography [14]. The dopant is then diffused into sapphire wafers at $1700°$C for 1 hour in argon atmosphere, with rapid cooling to room temperature over 10 minutes, to ensure a high proportion of the Ti ion in its luminescent trivalent state. This process results in a peak titanium concentration of approximately 0.2 wt% Ti_2O_3 in Al_2O_3, and a diffusion depth of order 10 μm. While this is a high Ti concentration compared with commercial Ti:Sapphire laser systems, it results in a low refractive-index change and a weakly-confined waveguide mode. Diffusion of gallium into sapphire yields well-confined modes [13] and the combination of Ga diffusion for passive waveguides and Ti diffusion to provide gain may provide a route to optimizing both the waveguiding and spectroscopic aspects of the materials system. Both Ga and Ti in-diffusion in sapphire are adversely affected by a tendency to rapid (lateral) surface diffusion, which has been partially overcome by using ion beam milling for lateral definition of channel waveguides [26].

2.4. Ion beam implantation

For less than two decades, ion beam implantation has been used for the fabrication of waveguide laser structures in insulators. The first reported ion-implanted waveguide laser was a planar device produced in Nd:YAG [27].

Modifications of different nature – mechanical, chemical, and electronical – are induced during ion implantation in solids. Swift heavy ions passing through a material cause intense electronic excitations along the ion trajectory that may result in defect production or phase transformation on the nanometer scale. A dramatic decrease of the optical quality of the material has been reported in inert-gas (He, Ar, and Ne) implanted sapphire due to the formation of color centers [28]. To our knowledge, no sapphire or Ti:Sapphire waveguide has been produced by use of heavy-ion implantation and, despite several attempts of locally doping sapphire with Ti^{3+} through implantation, no waveguide operation was reported [29,30].

Also for light ions, the energy is transferred primarily by electronic excitation; however the induced damage is

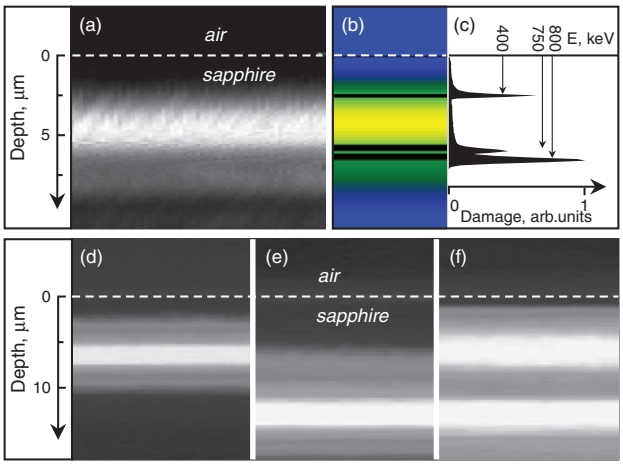

Figure 3 (online color at www.lphys.org) Mode patterns of 780-nm fundamental-mode laser light end-coupled to sapphire planar waveguides. (a) Experimental output profile recorded from a buried planar waveguide, (b) corresponding contour plot simulated with a simplified step-index profile estimated from (c) the accumulated damage profile calculated by SRIM simulations. Experimental output profiles recorded from two stacked planar waveguides. Individual excitation of (d) the upper and (e) the lower layer and (f) simultaneous excitation of both layers. The difference in the appearance of the upper guiding layer's width is due to different attenuation in front of the CCD camera. (Figure taken from [10])

less severe. Near the end of the ions' track, at lower energies, nuclear collisions predominate, leading to the displacement of lattice ions and resulting typically in a large cascade of damages. As a consequence, a (partial) amorphization of the material appears at the end of the ions' track, with a positive or negative refractive-index change depending on the ion fluence, the implanted material, and the nature of the interactions.

In the experimental example of Fig. 3a, successive implantations with significantly different energies produced an alternation of high and low refractive-index regions, resulting in a series of high-index layers in sapphire [10]. The dimensions and induced refractive-index changes were adjusted to permit fundamental mode propagation at 780 nm in a buried waveguide region, with a symmetric mode profile in the vertical direction optimized for coupling to a commercial 780-nm single-mode fiber, but prohibit light propagation in the superficial planar layer. A theoretical mode profile, Fig. 3b, was calculated with a simplified step-index profile, Fig. 3c. The experimental mode pattern, Fig. 3a, is in accordance with our theoretical calculation, Fig. 3b, both in terms of localization of the guided light in the buried planar waveguide and improvement of the mode symmetry in the vertical direction compared to surface waveguides [10]. Following the same approach of multiple energy implantations, stacked planar waveguides were fabricated by two double-implanted barriers. This procedure creates a superficial and a buried planar waveguide. The output profiles recorded after end-coupling fundamental-mode laser light at 780 nm into the sample show that the upper and lower guiding layers can be excited individually, Figs. 3d and 3e, or simultaneously, Fig. 3f. Variation of the ion energy and implantation through a slit offer possibilities to fabricate complex and multiple guiding structures [10], thus providing large versatility to this fabrication method.

Lasing buried channel waveguides have been produced by proton implantation in Ti:Sapphire substrates [11]. Similar to undoped sapphire [10], proton irradiation in Ti:Sapphire results in a negative refractive-index change of the implanted zone. Therefore, buried channel waveguides have been fabricated by implanting regions of low refractive index surrounding the intended channel waveguide region. Implantations were performed with high energy protons of $0.5 - 1$ MeV and doses between 2×10^{16} and 4×10^{16} H^+/cm^2. Vertical confinement was provided with a lower and upper barrier resulting from uniform irradiations of the whole surface of the c-cut Ti:Sapphire substrate at different energies in order to produce a buried planar waveguide. Within the planar waveguide, horizontal confinement was obtained by successive irradiations through a slit on both sides of the intended channel. A better lateral confinement can be achieved by a vertically more uniform distribution of the refractive-index change within the side barriers. Therefore, irradiations with several angles of incidence were performed, resulting in vertically stacked low-refractive-index barriers. Several 5-μm-deep buried channel waveguides were fabricated with widths of 10, 15, and 25 μm [11].

2.5. Femtosecond-laser writing

Femtosecond-laser writing has first been reported as a fabrication method to create refractive-index changes and optical waveguides in glasses [31]. The energy deposited in the focus of the laser irradiation induces localized melting of the material. After a fast re-solidification, a higher-density region with positive refractive-index change is formed. Translation of the sample during irradiation results in a linear structure in which light can be guided.

Channel waveguides have been fabricated in Ti:Sapphire by using 1-kHz (150-fs) pulses from a Ti:Sapphire femtosecond laser centered at 790 nm [12]. The 10-μm-diameter focused beam was collimated with a microscope objective with a numerical aperture of 0.3. The energy per pulse was ranging from 0.5 to 6 μJ. Since sapphire is a close-packed lattice, the modified regions possess lower density and, hence, a decreased refractive index compared to the unmodified bulk material. Channel waveguiding was observed in regions adjacent to the irradiated regions, just at the boundary between damaged and undamaged zone. The physical process responsible for the refractive-index change, probably linked with density

variations due to mechanical stresses in the crystalline lattice, is not resolved at the moment.

The fact that irradiation of pure sapphire under the same conditions as Ti:Sapphire does not produce any damage demonstrates that the Ti^{3+} impurities in the lattice sensitize sapphire to femtosecond-laser irradiation. These comparative results suggest that either a multiphoton-absorption process that involves the dopants' absorption band occurs or that replacement of Al^{3+} by the larger Ti^{3+} ions induces structural changes in sapphire which are sensitive to femtosecond-laser irradiation.

3. Optical waveguide characterization

In this section, we discuss the characterization of the optical properties of the Ti:Sapphire waveguides created by the various different fabrication techniques. Knowledge of the refractive-index profile is essential to ensure operation on a single spatial mode and to enable the design of tightly confined modes for low-threshold operation. When laser operation is obtained the output guided modes can be characterized and the laser performance can also be used as a convenient method of assessing the waveguide propagation losses. Measurement of the waveguide losses in the planar format is notoriously difficult as the requirements of cutting and re-polishing the waveguides make simple cut-back measurements impractical. The typically short propagation lengths also tend to make many other methods inaccurate for low-loss waveguides. In contrast, the use of laser performance in assessing the waveguide loss is both accurate and relatively simple. It should be noted that if round-trip losses are to be restricted to around the $\sim 1\%$ level, a 2-mm-long waveguide (equal to the length of bulk crystal used in [3]) would require propagation losses of ≤ 0.1 dB/cm. In Ti:Sapphire, the losses would be due to both the normal waveguide scattering losses and re-absorption loss owing to the presence of Ti^{4+} and other defects. Optimized planar waveguide technologies have driven scattering losses to ~ 0.1 dB/cm or lower in many materials (e.g. [32]), but this has often taken considerable effort after much higher first-generation losses (e.g. [33]). Optimized bulk material now has re-absorption losses significantly lower than 0.1 dB/cm, but this may not be the case for materials either grown or in some way modified in order to obtain a waveguide.

3.1. Refractive-index profiles

The refractive-index profiles obtained by the different fabrication methods determine not only the modal properties of the waveguides, but resulting from the modal properties, also influence the propagation losses. Therefore, it is of great interest to understand the ways in which refractive-index changes are created and their local distributions. We have employed prism-coupling methods, digital holography, and mathematical calculations to evaluate the refractive-index changes induced by the different fabrication methods described above.

In PLD-grown planar waveguides, evaluation of the refractive-index difference between the Ti:Sapphire layers and the undoped substrates was carried out via prism coupling of a 800-nm Ti:Sapphire laser beam into the corresponding films. For this purpose, a right-angled rutile prism with a base angle of $39.92°$ was used. With this configuration, the modal intensity profiles were measured for a 7.1-μm- and a 13.3-μm-thick film with a doping level equivalent to 0.1 wt% Ti_2O_3 that were deposited onto an undoped sapphire substrate. The measurements indicated single-mode and double-mode propagation, respectively, and these values were consistent with an increase in the refractive index Δn of the order of $2 - 8 \times 10^{-4}$ from sapphire to Ti(0.1 wt%):Sapphire.

The refractive-index change of Al_2O_3 induced by the addition of Ti_2O_3 was also calculated using the Maxwell-Garnett equation [18]:

$$\frac{\varepsilon - \varepsilon_m}{\varepsilon + 2\varepsilon_m} = \Xi \frac{\varepsilon_i - \varepsilon_m}{\varepsilon_i + 2\varepsilon_m}\,, \tag{1}$$

where $\varepsilon_m^{1/2} = 1.7620$ (η_o) and 1.7540 (η_e) are the refractive indices of sapphire at 800 nm, $\varepsilon_i^{1/2} = 2.35$ is the refractive index of Ti_2O_3 at 500 nm, $\Xi = 7.1 \times 10^{-4}$ is the volumetric fraction for 0.1 wt% Ti_2O_3 in Al_2O_3 (assuming that substitution of a small fraction of Al_2O_3 by Ti_2O_3 does not induce any change in the lattice constants), and $\varepsilon^{1/2} = \eta$ stands for the refractive index of Ti:Sapphire. From Eq. (1) we deduce for a Ti:Sapphire film with a doping level of 0.1 wt% Ti an increase in the refractive index of the order of $\Delta n = 3.9 \times 10^{-4}$ compared to undoped sapphire. This value is in good agreement with the aforementioned experimentally obtained Δn, ranging from $2 - 8 \times 10^{-4}$.

In Ti-in-diffused sapphire waveguides, the Ti distribution and, hence, the refractive-index profile depends upon the width and thickness of the Ti_2O_3 diffusion source stripe and the time and temperature of the diffusion. For the diffusion conditions mentioned above, the peak titanium concentration of 0.2 wt% Ti_2O_3 in Al_2O_3 (at the centre of the surface of the waveguide) resulted in a peak refractive-index elevation of the waveguide over the substrate of $\sim 6 \times 10^{-4}$, which is in the same range as the values in the aforementioned PLD-grown films, and a diffusion depth of order 10 μm. Gallium diffusion has been found to yield a refractive-index elevation as high as $\sim 6 \times 10^{-3}$ due largely to the high solid solubility of gallium in sapphire.

In proton-implanted undoped and Ti-doped sapphire, refractive-index changes were characterized by m-lines spectroscopy [34]. This technique is based on the measurement of the effective refractive index of propagating modes excited by prism coupling of light. Only negative refractive-index changes were observed in proton-irradiated sapphire, with gradient shape and maximum refractive-index decrease of typically $0.5 - 1\%$, for irradiation with 1-MeV protons at a fluence of 10^{16} H^+/cm^2.

The damaged barriers were localized ~ 8-μm deep for 1-MeV protons, which is in good accordance with Monte-Carlo calculations of the probability of a target atom being displaced from its lattice site (TRIM calculations).

Femtosecond-laser-irradiation induced refractive-index modifications in Ti:Sapphire were characterized using the technique of digital holography [35]. Optical path differences measured perpendicularly to the irradiation direction on a thick slice of the sample revealed localized refractive-index changes in and surrounding the damaged regions. Positive and negative refractive-index changes in the order of 1×10^{-4} and -2×10^{-4} were determined directly above and inside the cigar-like damaged zone, respectively.

3.2. Guided-mode profiles and luminescence output

The modal properties of the waveguides influence the pump-coupling efficiency, the output-beam quality, the pump-signal overlap, as well as the propagation losses, especially in cases where the refractive-index interface or the surroundings of the waveguide regions are lossy. We have characterized output-intensity profiles of all the different waveguide types.

The fluorescence characteristics of the pulsed-laser-deposited Ti:Sapphire waveguides were examined with an argon-ion pump laser operating on all lines. The fluorescence emission that was collected from the exit face of the waveguides was passing through an OG 550 filter to block the residual transmitted pump irradiation and subsequently imaged onto a beam profiler. The 11-μm-thick Ti:Sapphire planar waveguide that served as a host for the ribs, supported one mode in the guided direction and was multi-mode in the non-guided direction. A fluorescence intensity profile originating from a rib with a width of 10 μm and a height of 5 μm, which was fabricated in the Ti:Sapphire host via photolithographic patterning and subsequent Ar-ion milling, is shown in Fig. 4a. The profile indicates strong optical confinement, and the single-transverse-mode nature of the fluorescence was confirmed by measuring the beam-propagation factors (M^2) with a Coherent Modemaster beam propagation analyzer, resulting in values of 1.12 and 1.16 for the parallel and the perpendicular directions, respectively. Fig. 4b shows the luminescence output power from waveguides with different widths as a function of the input power. The maximum output powers were 283 μW ($w = 16$ μm), 243 μW ($w = 14$ μm), and 181 μW ($w = 10$ μm), and the corresponding slope efficiencies were 9.5×10^{-5}, 8.1×10^{-5}, and 6.2×10^{-5}.

The Ti-in-diffused waveguides fabricated as described in section 2.4 above were mono-mode at the lasing wavelengths from 775 nm to 805 nm, and multi-mode at pump wavelengths of 476 nm and 488 nm. The guided-mode intensity profiles in the TM polarization for a typical

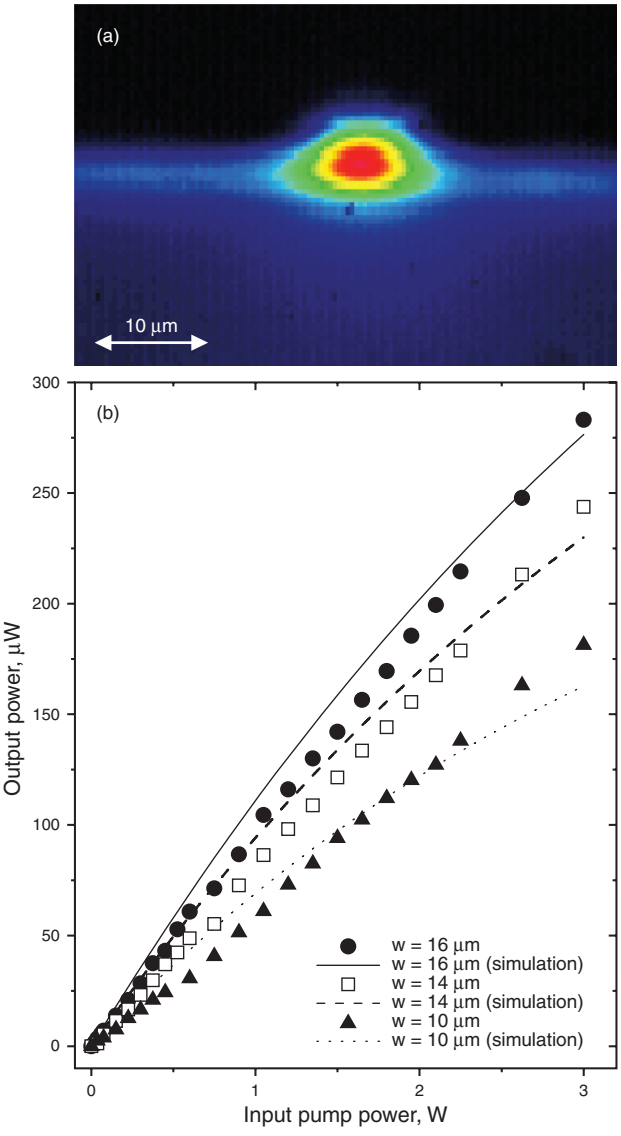

Figure 4 (online color at www.lphys.org) (a) Fluorescence emission profile from a Ti:Sapphire rib waveguide with depth of 5 μm and a width of 10 μm. (b) Fluorescence power as a function of pump power from an Ar^+ laser for 5-μm-deep ribs with a width at the bottom of: • – 16, □ – 14, and ▲ – 10 μm. The full line refers to the calculated fluorescence output for a rib with a width of 16 μm, the dashed line to 14 μm, and the dotted one to 10 μm. For the calculations, we assume 5-μm-deep ribs. (Figures taken from [8])

waveguide show a full mode size at half peak intensity of 5 μm×11 μm at $\lambda = 800$ nm and 4 μm×7 μm at $\lambda = 514.5$ nm. Ultimately, smaller spot sizes are desirable to achieve lower pump-power thresholds in waveguide devices. Gallium diffusion, where modal spot sizes of 2 μm ×2 μm are readily achieved, offers a promising route to lower thresholds.

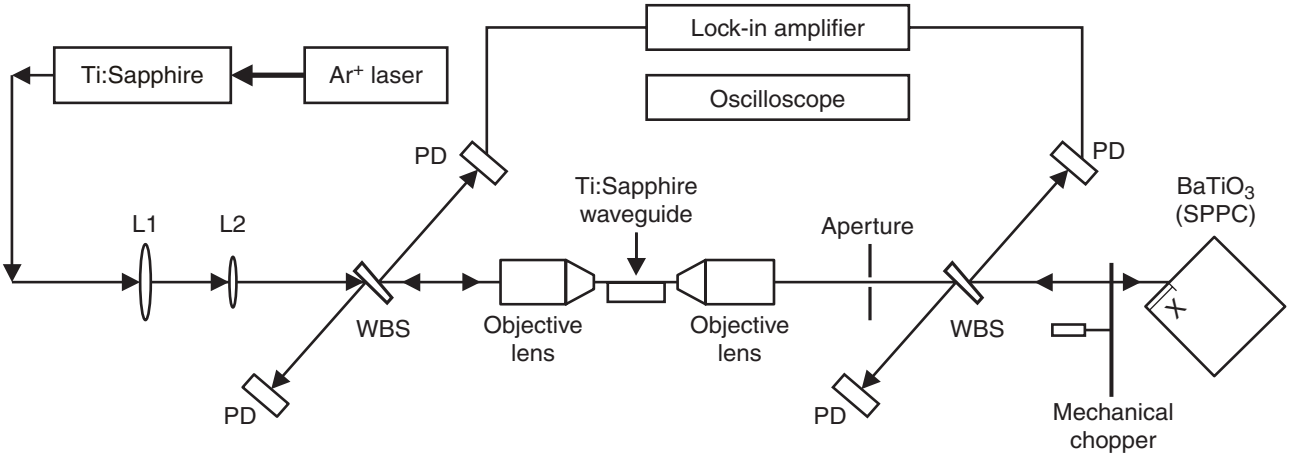

Figure 5 Typical experimental set-up for loss measurements with the self-pumped phase conjugation (SPPC) technique. L1 and L2 correspond to the cylindrical lenses of the telescope arrangement, WBS denotes the wedged beam splitters, PD stands for the photodiodes and x is the distance of the incidence point of the out-coupled beam on the crystal from its face. (Figure taken from [8])

Proton implantation induces well-controlled refractive-index decreases, hence the guided regions are formed by writing low-refractive-index barriers around the intended guided regions, and their mode profiles can be easily adjusted by changing the implantation parameters and geometries. By choosing different channel dimensions and optical confinement in the horizontal and vertical directions, we produced elliptical fundamental-mode profiles, with larger modal fields in the horizontal direction. Also cylindrical mode shapes can be achieved by adjusting the implantation energies, doses, and geometries.

After femtosecond-laser irradiation in Ti:Sapphire, multimode propagation at $\lambda = 633$ nm with circular mode profiles was observed in 10-mm-long channel waveguides. Waveguiding was not dependent on polarization even if TE and TM propagating modes exhibited slightly different field distributions.

3.3. Propagation losses

The propagation losses of a waveguide provide an indication of the waveguide quality and set a lower limit for the pump-intensity threshold of waveguide laser operation. Accurate propagation-loss measurements are difficult to perform in waveguides, because cut-back measurements, which are routinely performed in fibers, are usually excluded owing to the need to repolish the cut surface between subsequent measurements. Alternative methods include the moving-prism-coupling method in case of planar waveguides or, in the case of channel waveguides, the self-pumped phase-conjugation method, fiber-coupling methods, streak-of-luminescence and streak-of-scattering measurements. In both sample geometries, a rather accurate method appears to be the measurement of pump-laser threshold versus output coupling.

An upper limit for the propagation loss in the PLD-grown Ti:sapphire planar waveguide laser was evaluated using Eq. (2), which provides the absorbed-pump-power threshold for lasing (P_{th}) as a function of the overlap of the pump and laser modes [36]:

$$P_{th} = \left(\frac{hc}{2\lambda_p \tau_{fl} \sigma_e \eta_q}\right)\left(\frac{\delta}{L}\right)\left(\frac{1}{J}\right), \qquad (2)$$

where h is Planck's constant, c is the speed of light, $\tau_{fl} = 3.2\ \mu$s is the fluorescence lifetime, $\sigma_e = 3.65 \times 10^{-19}$ cm^2 is the stimulated-emission cross-section, $\eta_q = 0.8$ is the pump quantum efficiency at room temperature, $\lambda_p = 501$ nm the wavelength of the Ar$^+$ pump laser (the average of the two strongest emission lines at 488 and 514 nm was assumed), δ is the round-trip loss, L is the laser cavity length and J is a volume integral describing the overlap of the normalised pump and laser modes and was calculated from the measured mode profiles. From Eq. (2), a loss of 1.8 dB/cm was deduced and was attributed to surface scattering originating from particulates that were present on the film. However, this value represents a "worst-case scenario" estimation, as it also accounts for losses due to imperfect cavity mirrors attachment and end-face polishing.

Due to its non-destructive nature the self-pumped phase-conjugation (SPPC) [37] method was routinely used for propagation-loss measurements in Ti:Sapphire channel waveguides. In a typical experimental configuration shown in Fig. 5, the 720-nm output from a Ti:Sapphire laser, was shaped by a cylindrical-lens telescope to achieve an aspect ratio that would fit the mode of each channel waveguide and thus ensure optimization of the input coupling [8]. The beam was then launched into and out-coupled from the waveguides using two microscope objectives. The output was subsequently phase-conjugated from

a nominally undoped $BaTiO_3$ crystal in a standard total-internal-reflection geometry. The response of the crystal was optimized by varying the transverse position of the beam input and the angle of incidence. The advantage of this technique is that the retro-reflected beam is automatically coupled back into the waveguide without any launch losses other than the Fresnel reflections, thereby enabling evaluation of the propagation-loss coefficient via measurement of its transmittance through the waveguide. The propagation loss for a rib waveguide with a cross-section of $10\ \mu\text{m}\times3.5\ \mu\text{m}$ produced via a combination of PLD and Ar-ion milling was 1.7 ± 0.1 dB/cm. This loss was comparable with the upper limit of 1.8 dB/cm obtained for the Ti:Sapphire planar waveguide host and thus suggested that the rib-fabrication process did not itself introduce any significant loss.

When measured with the same method, buried channel waveguides fabricated via proton implantation with cross-sections of $15\ \mu\text{m}\times5\ \mu\text{m}$ and $10\ \mu\text{m}\times5\ \mu\text{m}$ showed losses of 1.0 and 1.3 dB/cm, respectively, at 720 nm. The higher loss level of the narrower guides was due to the stronger interaction of the modal field with the optical barriers.

The propagation losses of Ti-in-diffused sapphire waveguides have been estimated from laser performance to be as low as 0.8 dB/cm at the lasing wavelength of 790 nm. Further optimization of the titanium-diffusion process to reduce surface roughness and lateral diffusion is expected to readily yield losses as low as 0.2 dB/cm.

Finally, in femtosecond-laser-written waveguides, propagation losses of $2.3 - 2.5$ dB/cm have been determined with two experimental methods, either by fitting the exponential intensity decrease along the streak of luminescence of Ti^{3+} ions or by measuring the output intensity with fiber coupling in a passive channel waveguide at $\lambda = 633$ nm.

4. Waveguide laser performance

In this section, we review the laser performance achieved to date in Ti:Sapphire waveguides. Although the laser performance of optimized bulk lasers cannot yet be matched, the attraction of a guided-wave source may still be considerable for specific devices such as parallel optical coherence tomography [38], integrated sensor technology, or compact, high-repetition-rate femtosecond-laser sources [17]. The continuing drive to lower propagation losses and strong optical confinement will also inevitably bring considerable improvement in laser performance from these first-generation devices.

4.1. Planar waveguide lasers

To our knowledge, the only successful operation of Ti:Sapphire waveguide lasers with a planar geometry has been reported for structures fabricated via PLD [5].

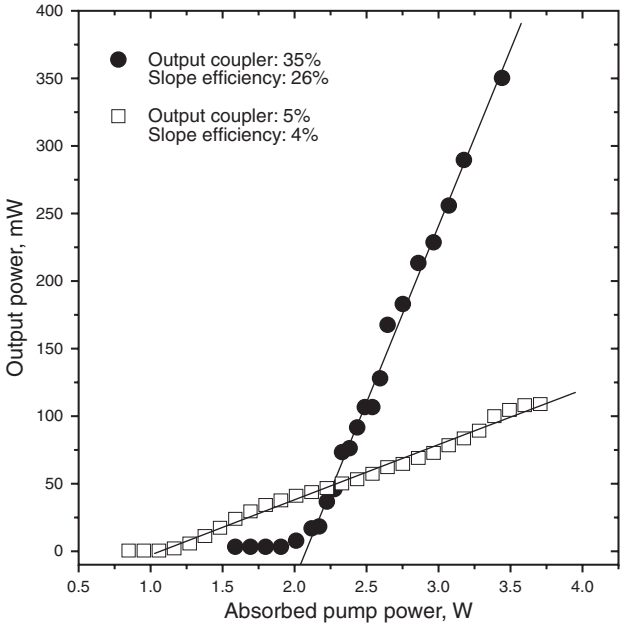

Figure 6 Laser performance of a PLD-grown Ti:Sapphire planar waveguide with a thickness of $12.3\ \mu$m for two output couplers with transmissions of 4% and 35% at the lasing wavelength. (Figure taken from [5])

The produced films were also suitable as broadband light sources for interferometric applications, providing spatially coherent, broadband (130-nm-FWHM) luminescence of several hundreds of microwatts of power when pumped with an Ar^+ laser with output powers up to 1 W [18,39].

Quasi-continuous-wave (CW) laser operation was obtained at room temperature at an absorbed-pump-power threshold of 720 mW [5]. Due to the larger stimulated-emission cross-section of the waveguides for the π- compared to the σ-polarization, the laser output was π-polarized regardless of the polarization state of the pump beam. Laser emission was centered near 808 nm. The spectral output as recorded by an optical spectrum analyzer (OSA) is characterized by spikes which represent an etalon effect from the cavity mirrors. A maximum output of 357 mW for 3.44 W of absorbed power and a slope efficiency of 26% were obtained using an output coupler with a transmission of 35% at the lasing wavelength. The output characteristics as a function of absorbed pump power are shown in Fig. 6, for two different values of output-coupler transmission.

4.2. Channel waveguide lasers

One of the motivations for our research on Ti:Sapphire channel waveguides is to develop a high-repetition-rate, short-pulse waveguide laser for applications in Optical

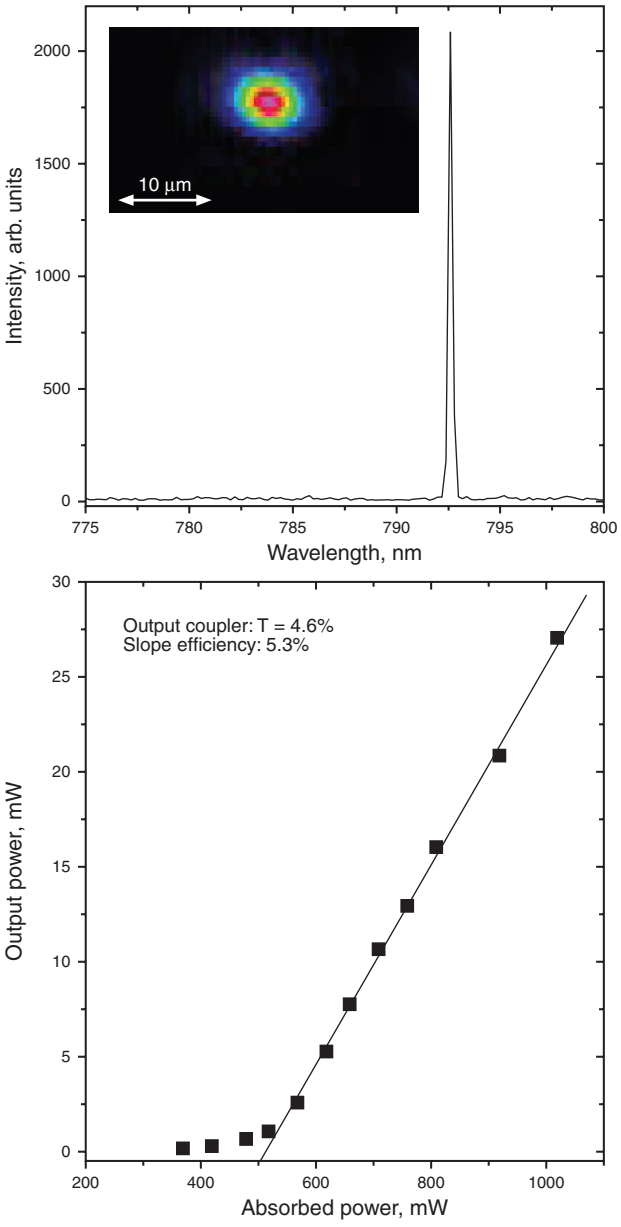

Figure 7 (online color at www.lphys.org) Lasing characteristics of a Ti:Sapphire rib waveguide with a cross section of 3.5 μm$\times$10 μm. (a) Lasing spectrum for an absorbed pump power of 350 mW. A laser mode profile originating from this structure is shown in the inset. (b) Output power versus the absorbed power for an output coupler with a transmission of 4.6%. (Figures taken from [9])

Coherence Tomography (OCT), where large-bandwidth, high-brightness light sources are required [40]. Apart from the possibility to achieve low laser thresholds as a result of the confinement of the laser and pump modes, channel geometries have also the potential to provide near-circular, single-transverse-mode beams. This latter point allows integration of channel waveguide lasers with the fiber-optic interferometers used in OCT systems. Ti:Sapphire waveguide lasers in channel format have so far been realized by photolithographic patterning and Ar-ion milling of PLD-grown layers [9], proton implantation [11], and thermal diffusion of Ti_2O_3 into sapphire [14].

The combination of photolithographic patterning and etching by Ar-ion beams produced rib waveguides in PLD-grown planar hosts [8], which were suitable as single-transverse-mode luminescence sources for OCT applications [38]. Laser operation in the ribs was demonstrated using an extended-cavity configuration [9]. This laser-resonator format allows introduction of intra-cavity elements for modulation or tuning, and elimination of losses resulting from a potential non-perpendicularity of the end-faces of the sample to the channels. The beam from the Ar^+ pump laser operating on all lines was coupled into the ribs using a microscope objective with a magnification of $\times 6.3$ after passing through an optical chopper. The latter was operating with a 8% duty cycle and was used to prevent any mirror damage via the pump irradiation. To form the cavity, a lightweight thin mirror with a reflectivity of 99.4% and transmission of 86% at the lasing and pump wavelengths, respectively, was attached to the input face of the sample. The output from the rib waveguides was collimated by a graded-index objective with a focal length of 14 mm before propagating towards the out-coupling mirror. To reduce losses, a 143-nm-thick single antireflection layer of MgF_2 (refractive index $n = 1.38$) was thermally evaporated on the out-coupling face. A set of two mirrors with transmission values of 0.8% (HR mirror) and 4.6% at the laser wavelength, were successively used as output couplers. The output passed through a filter to block any residual pump irradiation and was then directed onto a power meter or an OSA as required.

CW laser operation was demonstrated at room temperature and at an absorbed-pump-power threshold of 265 mW when the laser cavity was formed by two high-reflective (HR) mirrors. This threshold value for the ribs was more than a factor of two lower in comparison to their planar counterpart, for which the threshold was 560 mW [5]. Laser emission was observed at 792.5 nm and the recorded spectral output at an absorbed pump power of 350 mW is shown in Fig. 7a. When the HR output mirror was replaced by a 4.6% output coupler, the lasing threshold increased from 265 to 315 mW. The lasing characteristics obtained with this laser cavity are shown in Fig. 7b. The rib waveguide laser emitted 27 mW for 1 W of absorbed pump power, and a slope efficiency of 5.3% was obtained. Notably, this value is higher than the one obtained from the planar version of this waveguide (4%) [5]. Similar to the planar hosts, the laser output from the ribs was found to be π-polarized and a laser-mode profile originating from a rib with a cross-section of 10 μm$\times$3.5 μm for an absorbed pump power of 350 mW is shown in the inset in Fig. 7a. Measurements of the beam-propagation factors (M^2) showed diffraction-limited output with values of 1.3 and 1.2 for the parallel and the perpendicular directions with respect to the waveguide plane, respectively, in-

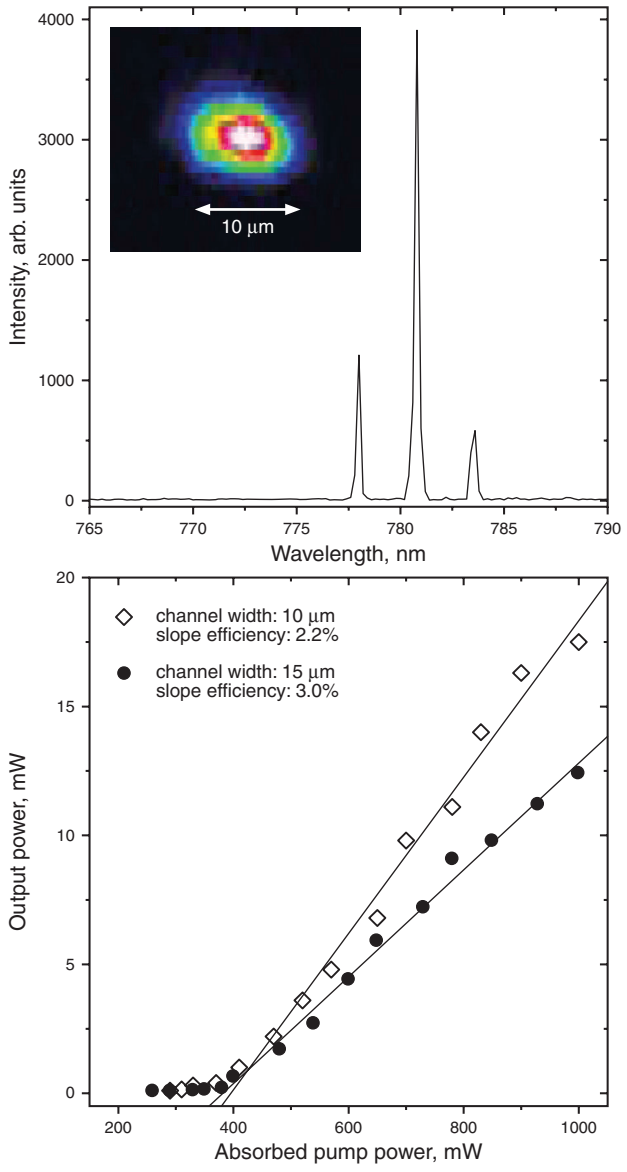

Figure 8 (online color at www.lphys.org) Lasing characteristics of proton-implanted Ti:Sapphire buried channel waveguides. (a) Lasing spectrum originating from a waveguide 5 μm and 10 μm in height and width, respectively. The corresponding laser mode profile is shown in the inset. (b) Dependence of the output power from two waveguide lasers with cross sections of 5 μm$\times$15 μm and 5 μm$\times$10 μm, respectively, as a function of the absorbed power for an output coupler with a transmission of 4.6%. (Figures taken from [11])

dicating single-transverse-mode laser emission. Ribs with widths above 20 μm were found to support at least two modes in the horizontal plane.

Lasing experiments with the Ti:Sapphire buried channel waveguides produced by proton implantation were performed at room temperature with an Ar^+ pump laser operating on all lines [11]. The laser resonator was formed by attaching at the end-faces two thin dielectric mirrors with high reflectivity and transmission at the lasing and pump wavelength, respectively. CW laser action was obtained in channel waveguides with a height of 5 μm and widths of 10 and 15 μm at absorbed pump power thresholds of 230 and 260 mW, respectively. Lasing was observed near 780 nm and the output was π-polarized regardless of the polarization state of the pump beam. Fig. 8a shows the laser spectral output together with a laser-mode profile (inset) originating from a channel with a width of 10 μm. The modulation in the spectrum is due to an etalon effect from the cavity mirrors and the sample, which was more evident at high pump powers. Measurements of the M^2 factors confirmed the near-diffraction-limited nature of the laser emission from the 10-μm-wide channels with values of $M_x^2 = 1.5$ and $M_y^2 = 1.2$ for the horizontal and perpendicular directions, respectively. The corresponding values for the 15-μm-wide channels were $M_x^2 = 2.5$ and $M_y^2 = 1.25$. By replacing the HR output mirror with one having a transmission of 4.6% at the lasing wavelength the threshold values increased to 260 and 290 mW for the 10- and 15-μm-wide channels, respectively. The laser input-output characteristics obtained with the 4.6% output coupler are shown in Fig. 8b. Slope efficiency values of 3% and 2.2% were obtained from the 15- and 10-μm-wide channels, respectively. The corresponding output powers are 17.5 and 12.4 mW for 1 W of absorbed power.

Lasing operation of the titanium-diffused sapphire channel waveguides was achieved with a pump wavelength of 514.5 nm at a pump power threshold of 210 $\pm$ 40 mW, and a slope efficiency value of 0.11% was obtained [14]. The laser cavity was formed by attaching to the end-faces two dielectric mirrors with high reflectivity at wavelengths between 760 nm and 810 nm. The lasers operated in quasi-CW mode for a wide range of pump duty cycles and laser emission was observed over a wavelength range of almost 50 nm, between 775 and 821 nm for pump powers up to 1050 mW. Spectral characteristics were very sensitive to the duty cycle and the pump conditions and wavelength switching was observed during laser emission, indicating temporal changes in the gain and loss in the laser cavity during pumping.

5. Conclusions

In recent years, Ti:Sapphire has served as one of the model systems to demonstrate the significant potential of optical waveguide lasers in doped dielectric crystalline materials. Fabrication methods such as pulsed laser deposition, reactive ion etching or Ar-ion milling, ion in-diffusion, and light-ion implantation have been explored successfully and surface and buried, planar and channel waveguide lasers have been demonstrated in Ti:Sapphire for the first time. Since the propagation losses of these first-generation waveguides are still rather high, substantial improvement is required in order to obtain ultra-low-threshold, tunable, and mode-locked waveguide lasers and to explore their

full potential as light sources in optical pumping, optical coherence tomography, spectroscopy, optical sensing, and other types of applications in integrated optics.

Acknowledgements The authors thank their colleagues P. Hoffmann, A. Crunteanu, V. Apostolopoulos, S. Rivier, C. Schnider, C.N. Borca, S. Bourquin, G. Jänchen, T. Colomb, C. Depeursinge, R.P. Salathé, C. Hibert, and H. v. Lintel from the Swiss Federal Institute of Technology, Lausanne, Switzerland, A.A. Anderson, L.M.B. Hickey, D.A. Sager, T. Bhutta, and T.C. May-Smith from the University of Southampton, United Kingdom, P. Moretti and J. Mugnier from the University of Lyon, France, R. Osellame, G. Cerullo, and P. Laporta from the Politecnico di Milano, Italy, Ch. Buchal and A. Petraru from the Forschungszentrum Jülich, Germany, and A.M. Kowalevicz, T. Ko, I. Hartl, and J.G. Fujimoto from the Massachusetts Institute of Technology, Cambridge, Massachusetts, United States for their contributions to the experiments and helpful discussions.

References

[1] P.F. Moulton, J. Opt. Soc. Am. B **3**, 125 (1986).
[2] R. Ell, U. Morgner, F.X. Kärtner, J.G. Fujimoto, E.P. Ippen, V. Scheuer, G. Angelow, T. Tschudi, M.J. Lederer, A. Boiko, and B. Luther-Davies, Opt. Lett. **26**, 373 (2001).
[3] A.M. Kowalevicz, T.R. Schibli, F.X. Kärtner, and J.G. Fujimoto, Opt. Lett. **27**, 2037 (2002).
[4] A.A. Anderson, R.W. Eason, M. Jelínek, C. Grivas, D. Lane, K. Rogers, L.M.B. Hickey, and C. Fotakis, Thin Solid Films **300**, 68 (1997).
[5] A.A. Anderson, R.W. Eason, L.M.B. Hickey, M. Jelínek, C. Grivas, D.S. Gill, and N.A. Vainos, Opt. Lett. **22**, 1556 (1997).
[6] M. Jelínek, R.W. Eason, J. Lančok, A.A. Anderson, C. Grivas, C. Fotakis, L. Jastrabík, F. Flory, and H. Rigneault, Thin Solid Films **322**, 259 (1998).
[7] A. Crunteanu, M. Pollnau, G. Jänchen, C. Hibert, P. Hoffmann, R.P. Salathé, R.W. Eason, C. Grivas, and D.P. Shepherd, Appl. Phys. B **75**, 15 (2002).
[8] C. Grivas, D.P. Shepherd, T.C. May-Smith, R.W. Eason, M. Pollnau, A. Crunteanu, and M. Jelínek, IEEE J. Quantum Electron. **39**, 501 (2003).
[9] C. Grivas, D.P. Shepherd, T.C. May-Smith, R.W. Eason, and M. Pollnau, Opt. Express **13**, 210 (2005).
[10] L. Laversenne, P. Hoffmann, M. Pollnau, P. Moretti, and J. Mugnier, Appl. Phys. Lett. **85**, 5167 (2004).
[11] C. Grivas, D.P. Shepherd, R.W. Eason, L. Laversenne, P. Moretti, C.N. Borca, and M. Pollnau, Opt. Lett. **31**, 3450 (2006).
[12] V. Apostolopoulos, L. Laversenne, T. Colomb, C. Depeursinge, R.P. Salathé, M. Pollnau, R. Osellame, G. Cerullo, and P. Laporta, Appl. Phys. Lett. **85**, 1122 (2004).
[13] V. Apostolopoulos, L.M.B. Hickey, D.A. Sager, and J.S. Wilkinson, Opt. Lett. **26**, 1586 (2001).
[14] L.M.B. Hickey, V. Apostolopoulos, R.W. Eason, J.S. Wilkinson, and A.A. Anderson, J. Opt. Soc. Am. B **21**, 1452 (2004).
[15] L.D. Morpeth, J.C. McCallum, and D.N. Jamieson, Nucl. Instrum. Methods Phys. Res. Sect. B **181**, 372 (2001).
[16] L.S. Wu, A.H. Wang, J.M. Wu, L. Wei, G.X. Zhu, and S.T. Ying, Electron. Lett. **31**, 1151 (1995).
[17] B. Stormont, I.G. Cormack, M. Mazilu, C.T.A. Brown, D. Burns, and W. Sibbett, Electron. Lett. **39**, 1820 (2003).
[18] M. Pollnau, R.P. Salathé, T. Bhutta, D.P. Shepherd, and R.W. Eason, Opt. Lett. **26**, 283 (2001).
[19] A. Crunteanu, G. Jänchen, P. Hoffmann, M. Pollnau, Ch. Buchal, A. Petraru, R.W. Eason, and D.P. Shepherd, Appl. Phys. A **76**, 1109 (2003).
[20] A. Crunteanu, P. Hoffmann, M. Pollnau, and Ch. Buchal, Appl. Surf. Sci. **208-209**, 322 (2003).
[21] J. Lančok, M. Jelínek, J. Bulíř, and P. Macháč, Laser Phys. **8**, 303 (1998).
[22] Y.J. Sung, H.S. Kim, Y.H. Lee, J.W. Lee, S.H. Chae, Y.J. Park, and G.Y. Yeom, Mat. Sci. Eng. **B82**, 50 (2001).
[23] S.H. Park, H. Jeon, Y.J. Sung, and G.Y. Yeom, Appl. Opt. **40**, 3698 (2001).
[24] I. Baumann, S. Bosso, R. Brinkmann, R. Corsini, M. Dinand, A. Greiner, K. Schafer, J. Sochtig, W. Sohler, H. Suche, and R. Wessel, IEEE J. Select. Topics Quantum Electron. **2**, 355 (1996).
[25] J. Amin, M. Hempstead, J.E. Roman, and J.S. Wilkinson, Opt. Lett. **19**, 1541 (1994).
[26] V. Apostolopoulos, D.A. Sager, J.S. Wilkinson, and L.M.B. Hickey, in: OSA Trends in Optics and Photonics, vol. 73, Conference on Lasers and Electro-Optics, OSA Technical Digest, Postconference Edition (Optical Society of America, Washington DC, 2002), p. 251.
[27] P.J. Chandler, S.J. Field, D.C. Hanna, D.P. Shepherd, P.D. Townsend, A.C. Tropper, and L. Zhang, Electron. Lett. **25**, 985 (1989).
[28] Y. Song, C.H. Zhang, Z.G. Wang, Y.M. Sun, J.L. Duan, and Z.M. Zhao, Nucl. Instrum. Methods Phys. Res. Sect. B **245**, 210 (2006).
[29] L.D. Morpeth and J.C. McCallum, Appl. Phys. Lett. **76**, 424 (2000).
[30] E. Alves, C. Marques, R.C. da Silva, T. Monteiro, J. Soares, C. McHargue, L.C. Ononye, and L.F. Allard, Nucl. Instrum. Methods Phys. Res. Sect. B **207**, 55 (2003).
[31] K.M. Davis, K. Miura, N. Sugimoto, and K. Hirao, Opt. Lett. **21**, 1729 (1996).
[32] C. Becker, T. Oesselke, J. Pandavenes, R. Ricken, K. Rochhausen, G. Schreiber, W. Sohler, H. Suche, R. Wessel, S. Balsamo, I. Montrosset, and D. Sciancalepore, IEEE J. Select. Topics Quantum Electron. **6**, 101 (2000).
[33] R.V. Schmidt and I.P. Kaminow, Appl. Phys. Lett. **25**, 458 (1974).
[34] R. Ulrich and R. Torge, Appl. Opt. **12**, 2901 (1973).
[35] E. Cuche, F. Bevilacqua, and C. Depeursinge, Opt. Lett. **24**, 291 (1999).
[36] M.J.F. Digonnet and C.J. Gaeta, Appl. Opt. **24**, 333 (1985).
[37] S. Brülisauer, D. Fluck, C. Solcia, T. Pliska, and P. Günter, Opt. Lett. **20**, 1773 (1995).
[38] S. Bourquin, L. Laversenne, S. Rivier, T. Lasser, R.P. Salathé, M. Pollnau, C. Grivas, D.P. Shepherd, and R.W. Eason, in: V.V. Tuchin, J.A. Izatt, and J.G. Fugimoto (eds.), Coherence Domain Optical Methods and Optical Coherence Tomography in Biomedicine IX, Proc. SPIE **5690**, 209 (2005).
[39] M. Pollnau, J. Lumin. **102-103**, 797 (2003).
[40] A.M. Kowalevicz, T. Ko, I. Hartl, J.G. Fujimoto, M. Pollnau, and R.P. Salathé, Opt. Express **10**, 349 (2002).